Asian Journal of Chemistry; Vol. 36, No. 2 (2024), 505-515

ASIAN JOURNAL OF CHEMISTRY

https://doi.org/10.14233/ajchem.2024.31089

A Hybrid Synthesis Approach: Tailoring Photocatalytic Activity of Co_3O_4 Nanoparticles by PEG Functionalization

ARSHDEEP KAUR[1], SANJEEV KUMAR[1,*], HARPREET KAUR[2,*], PRIT PAL SINGH[3,*], KHALID MUJASAM BATOO[4], JYOTI GAUR[5] and SUPREET[6]

[1]Department of Physics, Sri Guru Granth Sahib World University, Fatehgarh Sahib-140406, India
[2]Department of Physics, Chandigarh University, Gharuan Mohali-140413, India
[3]Department of Chemistry, Sri Guru Granth Sahib World University, Fatehgarh Sahib-140406, India
[4]King Abdullah Institute for Nanotechnology, King Saud University, Riyadh-11451, Saudi Arabia
[5]School of Basic and Applied Sciences, RIMT University, Mandi Gobindgarh-147301, India
[6]Amity School of Applied Sciences, Amity University Haryana, Amity Education Valley Gurugram (Manesar)-122412, India

*Corresponding authors: E-mail: kumarsanju25@gmail.com; mann.khant91@gmail.com; dhillonps2003@gmail.com

Received: 21 December 2023; *Accepted*: 19 January 2024; *Published online*: 31 January 2024; AJC-21540

This study presents a novel fusion of precipitation and hydrothermal methods for the synthesis of polyethylene glycol (PEG)-functionalized cobalt oxide (Co_3O_4) nanoparticles. The synthesized PEG/Co_3O_4 nanoparticles characterized using various techniques to elucidate their structure, composition, properties and application. The XRD analysis confirmed the formation of cubic phase of Co_3O_4 with a crystallite size of 2.04 nm. Two direct bandgap (E_g) transitions were observed at energy levels of 1.68 and 2.5 eV, exhibiting intensities that exceeded those reported in prior studies. The synthesized nanoparticles exhibited distinct structural features as revealed by FESEM and HRTEM investigations. Furthermore, the FTIR analysis provided evidence of interactions between PEG and Co_3O_4, suggesting successful functionalization. The high crystallinity of the PEG-mediated Co_3O_4 nanoparticles was further confirmed by the selected area electron diffraction (SAED) pattern. The XPS analysis revealed the presence of Co^{2+} and Co^{3+} ions, along with defect sites, confirming the successful synthesis of Co_3O_4 NPs with controlled oxidation states. These findings offer valuable insights into the chemical composition and electronic structure of the synthesized PEG-mediated Co_3O_4 nanoparticles. The photocatalytic activity of the PEG/Co_3O_4 nanoparticles was evaluated through the degradation of Congo red dye, a typical azo dye pollutant. The study revealed that PEG/Co_3O_4 (dose 200 mg L^{-1}) acted as an efficient photocatalyst for Congo red degradation. These results suggest that PEG-mediated Co_3O_4 nanoparticles hold promising potential as efficient photocatalysts for the treatment of wastewater containing organic contaminants.

Keywords: PEG-Co_3O_4 nanoparticles, Multi-structural form, Dye degradation, Hydrothermal, Photocatalytic activity.

INTRODUCTION

The dye industry has undergone a remarkable evolution in recent years, with the United States Colour Index now documenting tens of thousands of commercially available dyes. However, this progress comes with a significant environmental challenge. According to Liu *et al.* [1], global dye waste exceeds 60,000 tonnes annually, with azo dyes constituting a staggering 80% of this waste. Furthermore, certain azo dyes and their metabolites are known to be toxic and carcinogenic, raising serious concerns about their environmental impact. Textile effluents are a major source of dye pollution, with dye concentrations ranging from 10 to 800 mg L^{-1} [2]. This significant variability highlights the complex nature of dye pollution in textile wastewater. Different factories use diverse types and concentrations of dyes, making the problem multifaceted and requiring tailored solutions. The dyes employed in these industries not only pose threats to aquatic ecosystems and the organisms dwelling therein but also present serious risks to human health, including mutagenicity and carcinogenicity [3-5]. Addressing the pollution caused by industrial dyes necessitates advanced detection and removal techniques.

Traditional methods, such as precipitation, coagulation and flotation, have been utilized for the dye treatment [6], but

they come with significant drawbacks, including high chemical costs and environmental damage stemming from the byproducts of the treatment process. In response to these challenges, there has been a significant shift toward developing improved oxidation methods for dye degradation, with a focus on highly active photocatalysts. This approach is gaining prominence due to its cost-effectiveness, stability and environmental friendliness [7]. An advantageous characteristic of this photocatalytic approach is its ability to completely oxidize organic pollutants within a relatively short timeframe. Importantly, the process results in the mineralization of organic dyes into water, carbon dioxide and mineral acids, avoiding the generation of secondary pollution [8,9]. This innovative method represents a promising avenue for the efficient and environmentally friendly treatment of industrial dye effluents.

Among the plethora of photocatalysts, Co_3O_4 emerges as a particularly prominent nanomaterial, primarily owing to its exceptional photocatalytic capabilities, UV absorption characteristics and environmentally friendly behaviour [10]. Co_3O_4 nanoparticles exhibit remarkable photocatalytic activity, particularly when their size is reduced during the production process. Cobalt(II,III) oxide Co_3O_4 possesses a spinel structure and functions as a p-type semiconductor with a band gap ranging from 1.29 to 5 eV [11]. Co_3O_4 synthesis can be achieved through several processes, each offering unique advantages. These synthesis methods include co-precipitation [12], reflux [13], sol-gel [14], chemical spray pyrolysis [15], solvothermal [16], ball milling [17], hydrothermal [18] and more. The wide range of synthesis approaches highlights the versatility of tailoring Co_3O_4 nanoparticles for specific applications and desired properties. For instance, the sol-gel method [19] is recognized for producing high purity Co_3O_4, while hydrothermal synthesis allows for precise control over particle size and morphology [20]. The choice of synthesis method becomes crucial in determining the nanoparticle's characteristics and performance in different applications [21]. The tuneable band gap, spanning from 1.29 to 5 eV, allows for the customization of Co_3O_4 nanoparticles to suit specific requirements in different technological applications [22].

The surface engineering of Co_3O_4 nanoparticles plays a pivotal role in tailoring their properties for specific applications. Depending on the desired application, polymers and surfactants can be employed to generate a surface coating on Co_3O_4 nanoparticles [23]. Polymers exhibit significant influence over particle size and surface morphology, offering a means to finely tune the characteristics of Co_3O_4 nanoparticles [24]. These agents essentially serve as a protective layer, influencing the overall behaviour and functionality of the nanoparticles in various environments [25,26]. Polyethylene glycol (PEG) stands out as a particularly noteworthy polymer in this context. In addition to being non-flammable and non-toxic, it is also very easy to use, which contributes to its widespread use as a surfactant. Studies have demonstrated that PEG, with its consistent and ordered chain structure, readily adsorbs at the surface of metal oxide colloids, including Co_3O_4 nanoparticles. When PEG is adsorbed onto the colloid's surface, it significantly diminishes the colloid's activities and constrains the development rate in specific aspects [27]. It was observed that there is a significant gap in the literature on the photocatalytic activity of PEG-capped Co_3O_4 nanoparticles. Despite several studies on the photocatalytic characteristics of PEG-mediated ZnO [28,29] and TiO_2 [30,31] nanoparticles, there is a significant lack of published work on the similar behaviour of PEG-mediated Co_3O_4 nanoparticles. Considering this, present study intends to provide unique insights by synthesizing Co_3O_4 nanoparticles using PEG as a stabilizing agent, with a focus on establishing their photocatalytic behaviour. In this pioneering work, a simplified precipitation-cum-hydrothermal approach is used to synthesize multi-structured Co_3O_4 nanoparticles functionalized with PEG. This novel method enables the simple and one-step synthesis of unique nanostructured Co_3O_4. The resulting material exhibits exceptional efficiency in the degradation of toxic Congo red dye.

EXPERIMENTAL

Chime Pvt. Ltd. supplied cobalt acetate tetrahydrate (purity grade ≥ 99%), sodium hydroxide pellets (purity grade ≥ 99%) and polyethylene glycol-4000 (PEG-4000), all of which were used without further purification. Ethanol (purity ≥ 99%) was used to wash the precipitates and distilled water was used for the preparation of the solutions.

Synthesis of Co_3O_4 nanoparticles: To initiate the experimental process, a solution of cobalt acetate tetrahydrate, with a concentration of 0.2 M in 50 mL, was prepared according to the established protocol [32]. Subsequently, 30 mL of 0.01 M PEG solution was introduced into the solution. The resulting mixture underwent agitation for 1 h at 100 ºC, maintaining a pH level of 8.5. This step was crucial as the incorporation of PEG solution played a pivotal role in enhancing the solubility of solution and preventing the undesirable agglomeration of particles. The unique crosslinked structure inherent in the polymeric material derived from this process imparted exceptional resistance to chemical degradation. Following the solution preparation and agitational phase, the composite mixture was transferred into an autoclave and subjected to a 4 h baking period at 350 ºC. This autoclaving step conducted under elevated temperature and pressure conditions facilitated the crosslinking of polymer chains, thereby augmenting the material's overall texture. The final product showed an exceptional stability and durability exhibiting impressive thermal and mechanical characteristics. After the autoclaving process completed, the system was allowed to cool down to room temperature, resulting in the formation of solid particles of the treated material. The precipitates were carefully gathered and then subjected to an exhaustive purification procedure. After multiple ethanol and distilled water washes, the precipitates were dried at 80 ºC for 4 h. After crushing the black precipitates with a pestle and mortar, the powder was stored for further studies.

Characterization: The X-ray diffraction (XRD) study was conducted to evaluate the crystallite size and phases. The analysis was done using an X'PERT PRO apparatus from Panalytical in Japan, over the range of 10-90º 2θ. The determination of the energy band gap (E_g) of Co_3O_4 nanoparticles was carried out by UV-visible absorption spectral analysis. This spectrum

was performed using a UV-visible spectrophotometer (UV-2600, Shimadzu, Japan). A Carl Zeiss SUPRA 55VP field emission scanning electron microscope (FESEM) was used to examine the morphology of the synthesized nanoparticle, whereas JEM-2100 high-resolution transmission electron micro-scopy (HRTEM) from JEOL in Japan was used to measure the nanoparticle's size, lattice characteristics and interplanar spacing. The elemental composition of the Co_3O_4 nanoparticles was determined using energy dispersive X-ray (EDX) spectroscopy (AZtec system, Oxford Instruments, USA). The functional groups of the surface of Co_3O_4 nanoparticles was conducted using FTIR spectroscopy using an Alpha II instrument, Bruker, Germany in the wavenumber range from 4000 to 500 cm^{-1}. The Raman spectroscopy technique, specifically using the XploRA™ PLUS instrument manufactured by HORIBA in Japan, was utilized to investigate the properties and attributes of Raman phonon modes.

RESULTS AND DISCUSSION

Structural studies of PEG/ Co_3O_4 *via* X-ray diffraction (XRD): The XRD analysis of as-prepared PEG/Co_3O_4 sample (Fig. 1) provides insights into its crystal structure and phases. The XRD pattern in Fig. 1a shows strong conformity of all peaks with the standard cubic Co_3O_4 exhibited that the sample is well-crystallized [33,34]. The XRD patterns exhibit a small prominent peaks which might be due to the formation of CoO as trace element. In Fig. 1a, the prominent peaks matched with the spinel Co_3O_4 phase in the F*d3m* space group (JCPDS file No. 01-074-1657). This alignment further supports the favourable formation of Co_3O_4. Specifically, the peaks at 31.6534º, 37.2464º, 38.9804º, 45.2704º, 56.0654º, 59.7204º, 65.5854º and 68.0504º correspond to the (220), (311), (222) (400), (422), (511), (440) and (531) planes of the cubic Co_3O_4, respectively. To assess the crystallite size of Co_3O_4 nanoparticles, the strongest peak (311) was utilized and its size was determined to be 2.04 nm using Scherrer's equation [35]:

$$D = \frac{K\lambda}{\beta\cos\theta} \quad (1)$$

where D represents the average particle size of crystallites, λ is the X-ray wavelength, β is the full width at half maximum (FWHM) of the peak and θ is the Bragg's angle.

The X-ray pattern of the synthesized Co_3O_4 nanoparticles displayed distinct peaks with both sharp and fine widths, affirming the high crystallinity [36]. The PEG/Co_3O_4 nanoparticles have extremely tiny crystallite sizes as shown in Table-1. This observation may be attributed to several factors. For example, addition of polyethylene glycol (PEG) to the synthesis process may reduce crystallite size, since PEG stabilizes and controls nanoparticle development, resulting in finer architectures [37]. Additionally, the interaction between PEG and the Co_3O_4 nanoparticles may influence the nucleation and growth processes, resulting in reduced crystallite sizes [38]. The presence of PEG molecules on the nanoparticle surfaces can act as capping agents, hindering the agglomeration of particles and promoting the formation of smaller crystallites [39].

TABLE-1
CRYSTALLOGRAPHIC PARAMETERS OF PEG@CO_3O_4

2θ (°)	FWHM (°)	FWHM (radians)	d-spacing	Crystallite size (D) (nm)
31.6534	6.95640	0.12141	2.82442	1.24
37.2464	2.06997	0.03613	2.41214	4.23
38.9804	3.28100	0.05726	2.30874	2.68
45.2704	12.27400	0.21422	2.00149	0.73
56.0654	4.33500	0.07566	1.63902	2.17
59.7204	4.43700	0.07744	1.54714	2.16
65.5854	4.23300	0.07388	1.42226	2.33
68.0504	12.18900	0.21274	1.37662	0.82
D (average) = 2.04 nm				

UV-visible studies: In Fig. 2a, the UV-visible absorption spectrum of PEG-mediated Co_3O_4 nanoparticles is presented, spanning the wavelength range of 250-800 nm. The absorption

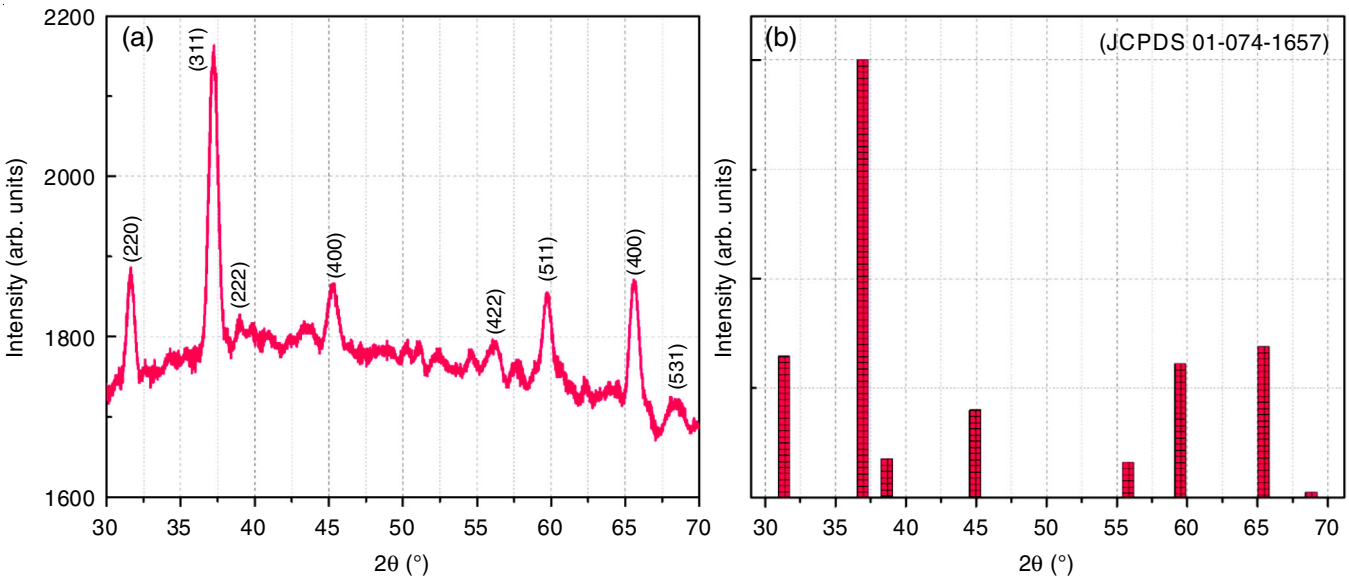

Fig. 1. XRD spectra of as-synthesized Co_3O_4 nanoparticles (a) and standard JCPDS (b)

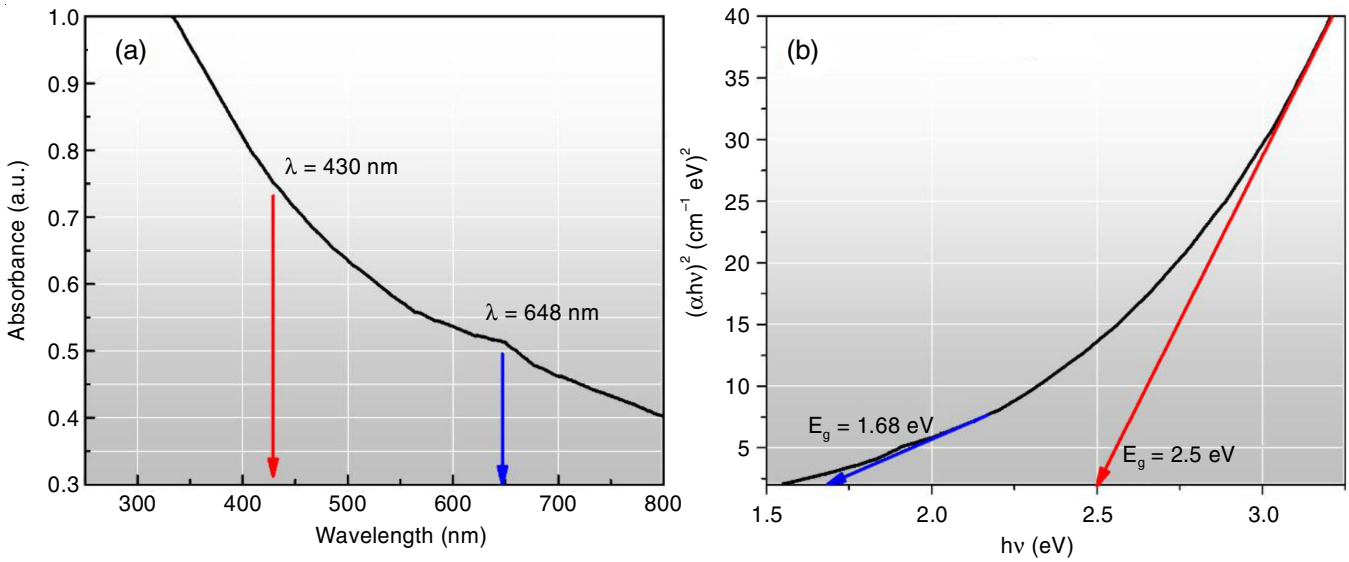

Fig. 2. Electronic band structure analysis of PEG-decorated Co_3O_4 nanoparticles (a) UV-visible absorption spectrum and (b) Tauc's plot for optical band gap energy

spectra exhibit distinct excitonic absorption bands at 430 and 648 nm, corresponding to $O^{2-} \rightarrow Co^{2+}$ and $O^{2-} \rightarrow Co^{3+}$ ligand-to-metal charge transfer (LMCT) bands [40]. The absorption peak at 400 nm signifies the formation of a significant number of Co^{2+}–O tetrahedrons, while the absorption at 680 nm suggests the development of Co^{3+}–O tetrahedrons as reported by He *et al.* [41]. The LMCT bands show significant changes when compared to previously reported synthesis methods. The conventional chemical precipitation methods for the synthesis of Co_3O_4 nanoparticles as reported by Dubey *et al.* [42], displayed LMCT bands at 528 and 785 nm. In contrast, the PEG/ Co_3O_4 nanoparticles in our study exhibit a blue-shifted absorption peak, moving from 528 to 430 nm for the first absorbance band and from 785 to 648 nm for the second. This shift in peak location provides the valuable insights into the size, crystallinity and imperfection existence of the synthesized nanoparticles. The observed blue shift in wavelength indicates a reduction in size and an enhancement in crystallinity for the PEG-decorated Co_3O_4 nanoparticles [43].

Although there are no visible peaks in the optical spectrum, which is a typical feature of Co_3O_4 nanoparticles since they do not exhibit strong *d-d* transitions, which are responsible for the visible absorption in transition metal complexes, the work focuses on calculating the band gap energy. Utilizing the UV-vis spectroscopy and Tauc's approach [44], the optical band gap energy (E_g) of Co_3O_4 was determined (Fig. 2b). Two direct E_g transitions were identified at 1.68 and 2.5 eV, surpassing the intensity reported for Co_3O_4 nanostructures in previous study [45]. The current work further investigates the electronic structure of Co_3O_4 nanoparticles, emphasizing the Co(II) and Co(III) coordination and the distribution of orbitals in the valence and conduction bands.

The structural composition of Co_3O_4 nanoparticles with a spinel structure involves one-third of cobalt atoms having tetrahedral oxygen coordination as Co(II), while the remaining two-thirds exhibit octahedral oxygen coordination as Co(III) [46]. Understanding the electronic configuration is crucial in elucidating the behaviour of the material. The 3*d*-orbitals of Co(III) comprise three T_{2g} levels and one e_g level, whereas those of Co(II) consists of two e_g levels and three T_{2g} levels. The intricate interplay of O_{2p} levels with the e_g and T_{2g} orbitals of both tetrahedral Co(II) and octahedral Co(III) contributes to the formation of valence band (VB) of Co_3O_4. Specifically, the valence band is dominated by O_{2p} orbitals, highlighting the role of oxygen in the electronic structure. Simultaneously, the conduction band (CB) comprises T_{2g} orbitals of tetrahedral Co(II) and e_g orbitals of octahedral Co(III). In this arrangement, the T_{2g} of Co(II) 3*d*-orbital emerges as the dominant CB orbital [47].

The distinctive two-energy band gap of Co_3O_4 nanoparticles reflecting the ability of cobalt to contribute eight electrons for nanoparticle formation, positions PEG-mediated Co_3O_4 nanoparticles as promising photocatalysts. The wide band gap energies of these nanoparticles make them suitable for various photocatalytic and photo-responsive applications suggesting enhanced photocatalytic activity due to their ability to absorb more UV-visible light [48].

FTIR studies: In Fig. 3a-c, the FTIR spectra of PEG, cobalt acetate and PEG-capped Co_3O_4 nanoparticles are presented, shedding light on the molecular interactions and functional groups present in each sample. In the FTIR spectrum of PEG, a broad absorption band in the range of 3800-3300 cm^{-1} is indicative of H-bonded O-H stretching (Fig. 3a) [49]. This region highlights the presence of hydroxyl groups in PEG indicating its hydrogen bonding capabilities. Additionally, a band at 2925 cm^{-1} corresponds to C-H bond stretching, while the C-O-C stretching vibration is evidenced by peaks at 1349-1089 cm^{-1} [50]. These characteristic peaks confirmed the molecular structure of PEG. The FTIR spectrum of cobalt acetate reveals the significant absorption bands corresponding to its molecular structure. The asymmetric and symmetric carbonyl stretching vibrations are observed at 1688 and 1545 cm^{-1}, respectively, indicating the presence of acetate groups. The Co-O stretching

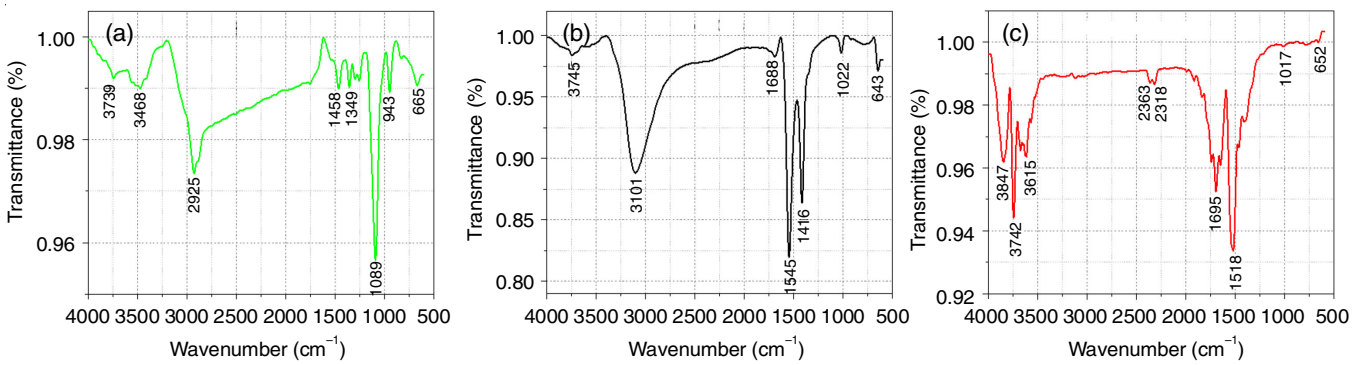

Fig. 3. FTIR spectra of (a) PEG in distilled water, (b) cobalt acetate in distilled water and (c) PEG-mediated Co_3O_4 nanoparticles

vibration is evident at 643 cm^{-1}, providing information about the cobalt-oxygen bonding in the acetate complex [51,52]. Furthermore, the broad band at 3300-2800 cm^{-1} is attributed to H-bonded O-H stretching, which is like due to the presence of water molecules associated with cobalt acetate [53]. In the FTIR spectrum of PEG-capped Co_3O_4 nanoparticles, the peak at 652 cm^{-1} is associated with the Co-O stretching of Co^{3+} ions trapped in the octahedral site, confirming the presence of cobalt oxide in the synthesized nanoparticles [54]. Moreover, the peaks at 3650-3450 cm^{-1} correspond to the O-H stretching of PEG [55], reinforcing the attachment of PEG molecules to the nanoparticle surface. Also, the peaks at 1695 and 1518 cm^{-1} are attributed to the carbonyl stretching of acetate moiety of Co_3O_4, further confirming the successful capping of Co_3O_4 nanoparticles with PEG.

Topographical studies: FESEM with an EDAX detector was used for the microanalysis of PEG-mediated Co_3O_4 nanoparticles, *i.e.* the texture and its assembly at various magnifications. FESEM image displays a 2D image that provided insight into the surface texture of PEG/Co_3O_4, elucidating the features such as the exterior morphology of material at varying magnifications and the nanoparticles' orientation. The FESEM images of PEG/Co_3O_4 nanoparticles are shown in Fig. 4a-d, acquired at magnifications ranging from 10 to 100 kX. A FESEM image of PEG/Co_3O_4 NPs is shown in Fig. 4a with a 10 kX resolution. Clustering of nanostructures of varying sizes and shapes has been detected. The findings demonstrated that the chemical synthesis of PEG/Co_3O_4 nanoparticles yielded spherical particles with coated interconnecting stratified frameworks and average particle dimensions of a few nm. The FESEM magnification was increased from 10 to 30 kX (Fig. 4b) to have a better view of the aggregated nanoparticles (Fig. 4a). It revealed the irregularly shaped nanoclusters formed by the accumulation of the spherical particles. At higher magnification, the FESEM image revealed distinct nanoclusters comprised of spherical particles (Fig. 4c-d). The Co_3O_4 nanoparticles exhibit comparable morphologies but possess significantly larger particle sizes [56,57]. The addition of the surfactant PEG to cobalt salt has altered the size of the resulting PEG/ Co_3O_4 nanoparticles. The physical action between Co_3O_4 and the PEG ion precipitates out uniformly sized and shaped spherical nanoparticles [58]. The cationic side of PEG and the cobalt species' positive end are electrostatically repelling one another. PEG molecules form a bilayer on the surface of Co_3O_4 to neutralize the electrostatic repulsion, resulting in the formation of Co_3O_4 nanoparticles [59]. The Co_3O_4 nanoparticles may be capped by the positively charged PEG ions, preventing them from growing laterally or changing shape from spherical (Fig. 4c-d). The average diameter of the crystallized size of annealed samples is about 20 nm. Similar to the reported PEG-assisted Co_3O_4 nanoparticles using the sol-gel method, tiny structures were identified in the current investigation [60-62]. PEG coatings surrounding the Co_3O_4 nanoparticles prevent agglomeration and allow for more precise sizing control.

As shown in the inset of Fig. 4a, Co_3O_4 nanoparticles were subjected to EDAX analysis and are composed of 69.44% cobalt and 30.56% oxygen by atomic weight. Only the surface functional groups have an impact on biosorption, whether it comes to physical or chemical characteristics. The results raise the possibility that cobalt and oxygen contribute to the significant photocatalytic activity by sequestering the dye molecules.

Morphological studies: The TEM image reveals the nanoparticle clusters (Fig. 5a). More detailed images were acquired to better portray the particle morphologies (Fig. 5b-d). The average nanoparticle size determined from the particle distributions was 15 nm. Analyses using SEM and TEM techniques showed that the synthesized Co_3O_4 nanoparticles were roughly spherical in form and varied in size from 10 to 18 nm [61]. In the synthesis process, during the early stages of Co salt reduction, the tiny Co nanoparticles expanded to generate bigger Co nanoparticles. These particles quickly turned into CoO particles, which kept ending up bigger in the solution. As the amount of surfactant varied, they evolved into distinct forms and sizes. Earlier study describes the shape-selective CoO nanoparticle synthesis using polyvinyl alcohol (PVA) as a capping [63]. However, polymerization of PVA at higher concentrations may result in the formation of templates that facilitate the development of anisotropic nanosheets or nano dendrites.

The appearance of discrete lattice fringes in the HRTEM image at high magnification (600 kX) is an indicative of the formation of extremely crystalline Co_3O_4 revealing the 0.25 nm *d*-spacing of the atomic planes. The monocrystalline character of PEG/CO_3O_4 was verified by the presence of a single crystallite. Fig. 5f depicts a TEM micrograph of the SAED pattern of the PEG/Co_3O_4 in dark field diffraction mode. It displays a flawless single crystal pattern with first-, second- and third-

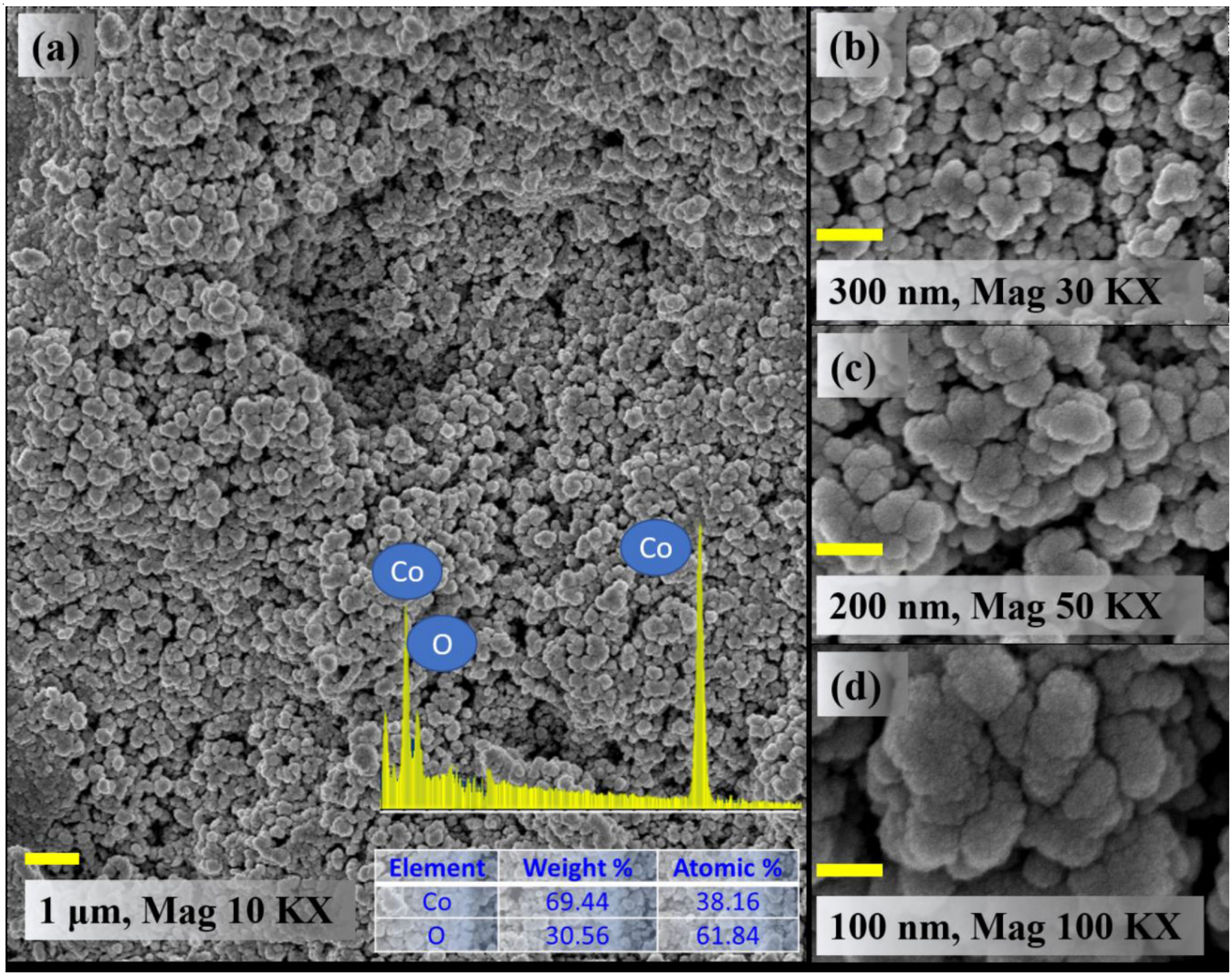

Fig. 4. FESEM images of PEG/Co_3O_4 NPs: (a) 10 kX, (b) 30 kX, (c) 50 kX and (d) 100 kX

order nanostructure facets and scattering of the circular arrangement, with brighter and clearer regions in the circles. This suggests that the crystals are in the nm range and are oriented randomly. The XRD spectrum of the PEG/Co_3O_4 nanoparticles and the corresponding electron diffraction spots depicted the same hexagonal crystal structure with space group *P*63*mc*.

X-ray photoelectron spectroscopy (XPS) studies: In this investigation, XPS technique was employed to scrutinize the valence states of elements at the surface of PEG-mediated Co_3O_4 nanoparticles. Fig. 6a reveals the elements presence on the surface of PEG-mediated Co_3O_4 nanoparticles and exhibited the distinct peaks corresponding to Co, C and O elements. Specific XPS peaks were identified, including Co (2s) at 926.58 eV, Co ($2p_{1/2}$) at 793.2 eV, Co ($2p_{3/2}$) at 777.96 eV, O (1s) at 529.4 eV, C (1s) at 283.07 eV, Co (2p) 134.60 eV, Co (3s) at 99.56.4 eV and Co (3p) at 57.21 eV [64,65]. The existence of each peak indicates the presence of the respective components and offers an insight into the surface chemistry. Two primary peaks are observed, arising from spin-orbit coupling ($2p_{1/2}$ and $2p_{3/2}$) (Fig. 6b). The binding energy of Co $2p_{3/2}$ peak at 778.31 eV indicates Co^{3+} in Co_3O_4 and Co $2p_{1/2}$ peak at 792.43 eV further supports the presence of Co^{3+} and confirmed the CoO formation [66]. Prominent peaks at 778.04 eV (Co $2p_{3/2}$) and 793.4 eV (Co $2p_{1/2}$) suggest the presence of Co ions in both +2 and +3 oxidation states [67], the absence of peak at 776.1 eV confirms the absence of metallic cobalt, which is consistent with the XRD and SAED findings.

Fig. 6d reveals a captivating four-peak structure in the O 1s spectrum, providing crucial insights into the chemical composition and surface characteristics of the material. The first peak O_I positioned at 527.90 eV corresponds to the strong metal-oxygen bonds, an indicative of Co-O linkages within the sample. The O_{ii} peak at 529.23 eV shows the presence of defect sites characterized by the minimal oxygen coordination [68]. These deviations from the ideal crystal structure could arise from missing oxygen atoms, vacancies or other structural imper-fections. Further analysis revealed the O_{iii} peak (530.16 eV), attributed to oxygen present in hydroxyl groups (-OH) [11]. This observation underlines the involvement of hydroxyl func-tionalities in the surface composition suggesting the presence of absorbed water molecules, adsorbed oxygen species or even surface oxides [69,70]. The presence of these

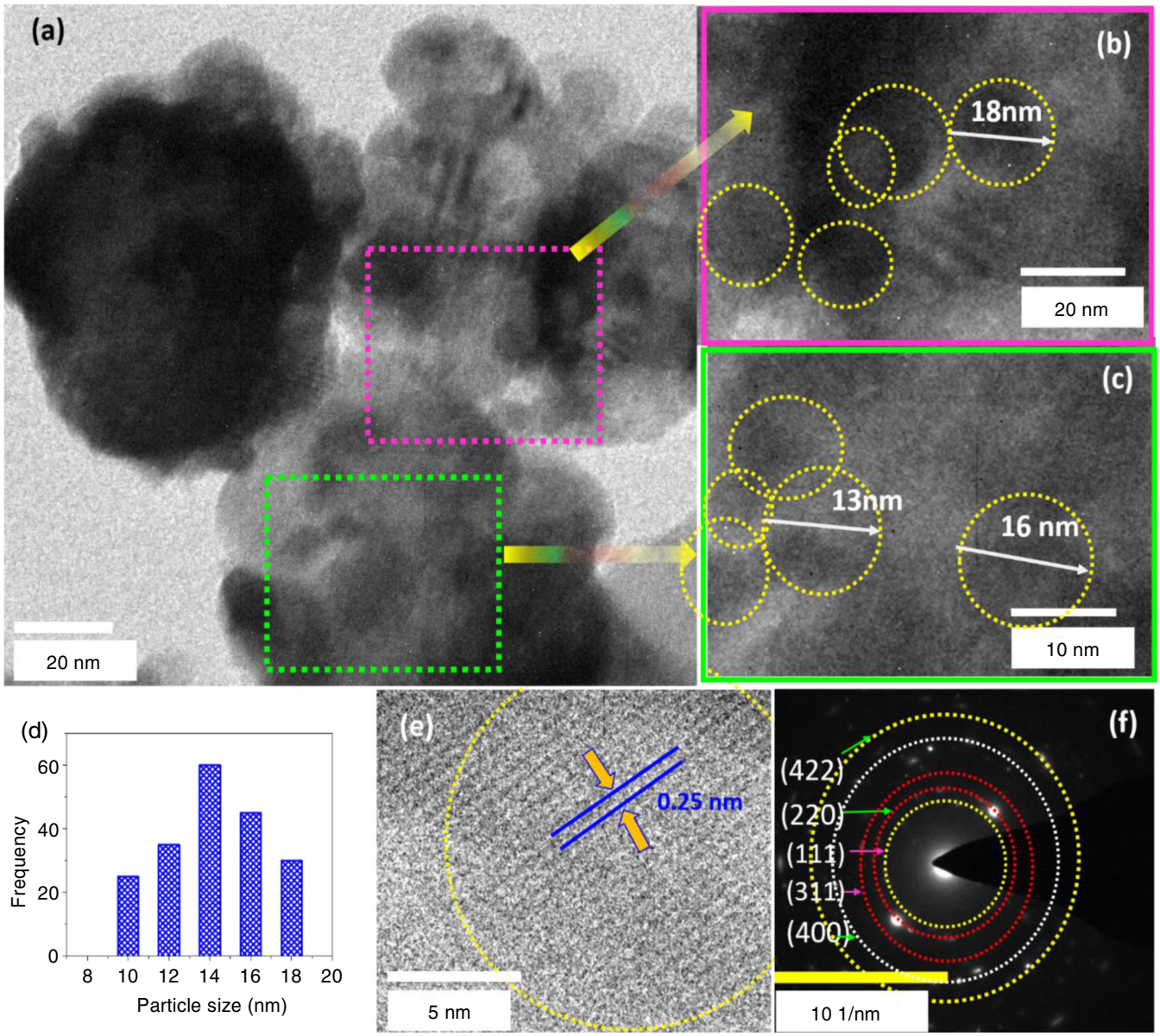

Fig. 5. Morphology of PEG-mediated Co_3O_4 nanoparticles: (a-c) HRTEM micrographs, (d) histogram of particle size distribution, (e) fringe patterns and (f) SAED patterns

groups can significantly influence the surface properties including wettability, surface acidity/basicity and catalytic activity. The O_{iv} peak (532.15 eV) sheds light on the interaction between the material surface and water molecules in its surrounding environment. This peak is associated with the oxygen content in physically adsorbed or chemisorbed water. Physical adsorption involves weak van der Waals forces, while chemisorption involves stronger chemical bonds. The intricate four-peak structure observed in the O 1s spectrum (Fig. 6d) has provided valuable insights into both the chemical composition and surface characteristics of the material under scrutiny. The XPS analysis provides strong evidence for the successful synthesis of Co_3O_4 nanoparticles with controlled oxidation states. The presence of both Co^{2+} and Co^{3+} ions, along with defect sites, suggests potential for further investigation and application in various fields.

Photocatalytic potential of Co_3O_4 nanoparticles

Degradation of Congo red dye: This study explores the complex field of photocatalysis, specifically examining the synthesized PEG-mediated Co_3O_4 nanoparticles and their impressive capacity to enhance the breakdown of azo dye Congo red dye. The existence of two stable aromatic rings intricately connected by the chromophore [71] adds to the complexity of Congo red, resulting in a strong resistance to degradation [72]. In order to establish a baseline, we examined the photostability of Congo red dye in the absence of a photocatalyst under ultraviolet light (Fig. 7a). Surprisingly, there was no significant decrease in Congo red dye concentration even after being exposed for 60 min. This observation clearly demonstrates that UV light alone has a negligible effect on changing the physical and chemical characteristics of the dye. Fig. 7b-c illustrate the photocatalytic process of the synthesized Co_3O_4 nanoparticles under various

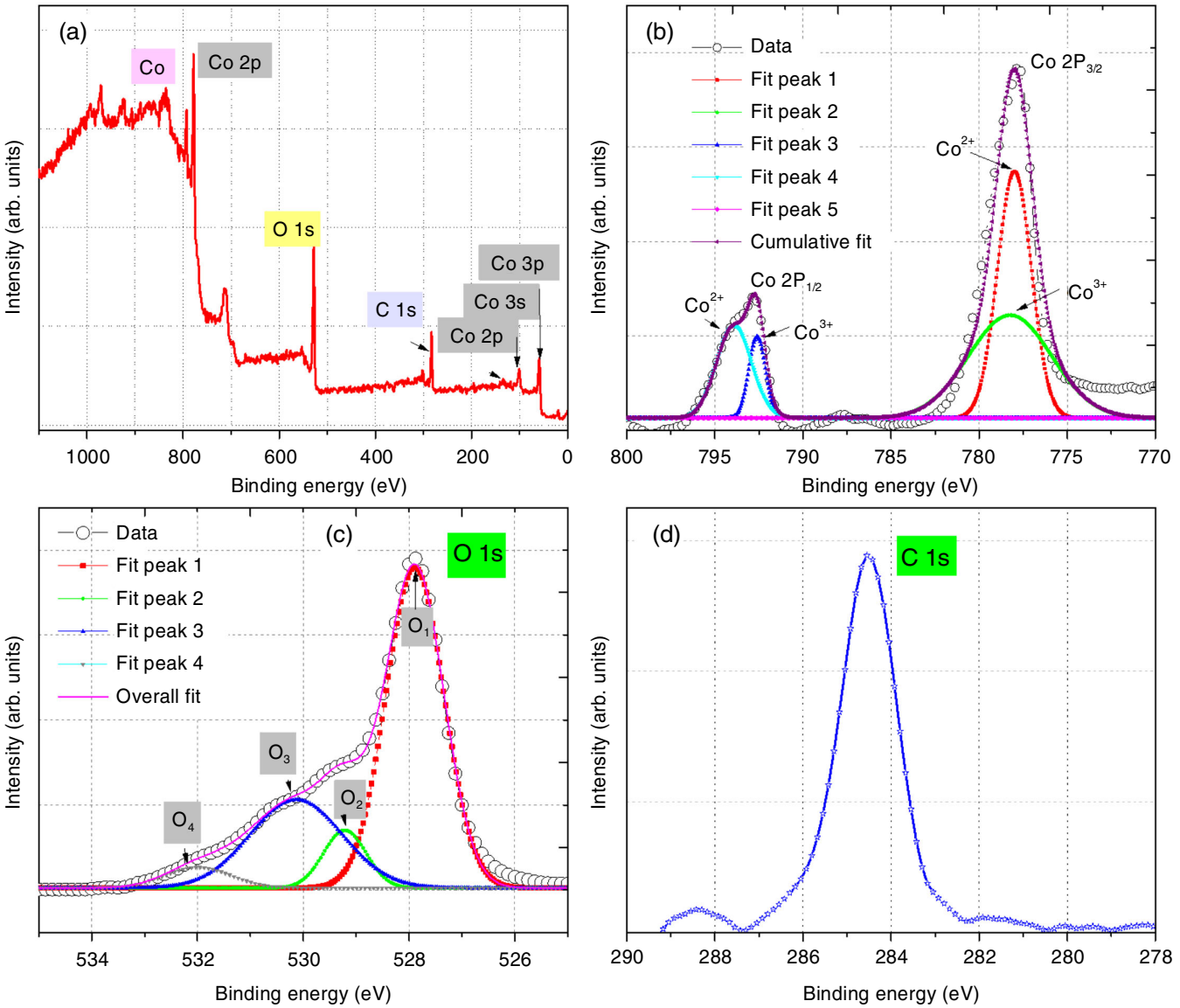

Fig. 6. XPS spectra of PEG-mediated Co_3O_4 nanoparticles: (a) Overview scan, (b) Co 2p spectrum, (c) O 1s spectrum and (d) C 1s spectrum

conditions. The results clearly depicted a steady decrease in Congo red dye concentration over time as evidenced by the diminishing peak at 501.2 nm in the UV-Vis spectra. After 150 min of UV irradiation, the peak disappears entirely indicating the complete degradation of Congo red dye. The visible colour of the solution change from original to transparent supports this observation. These results emphasize the crucial role of Co_3O_4 nanoparticles in facilitating the breakdown of the Congo red dye molecule. Fig. 7d delves deeper into the influence of Co_3O_4 nanoparticles dosage on the photocatalytic efficiency. In this study, higher dosages (150 and 200 mg L^{-1}) translated to a greater availability of active surface sites on the Co_3O_4 nanoparticles, thereby enhancing the degradation rate. An estimated degradation of 96.44% of the dye was achieved using a catalyst dose of 200 mg L^{-1}. This observation highlights the importance of optimizing the photocatalyst dosage for maximizing the photocatalytic efficiency.

Mechanism: The observed photocatalytic activity can be attributed to the generation of hydroxyl radicals ($^{\bullet}OH$) on the surface of PEG-mediated Co_3O_4 nanoparticles when exposed to UV-visible light. This phenomenon is supported by the well-established photocatalytic mechanism for metal oxides [73] (Fig. 8). Upon irradiation with UV light, electrons are excited from the valence band to the conduction band of Co_3O_4, creating electron-hole pairs (e^-/h^+). These energetic charge carriers then migrate to the surface of the nanoparticles, where they react with water and adsorbed oxygen molecules to generate active hydroxyl radicals:

$$^{\bullet}H_2O + h^+ \longrightarrow {}^{\bullet}OH + H^+$$

$$^{\bullet}O_2 + e^- \longrightarrow O_2^{\bullet-}$$

The highly reactive $^{\bullet}OH$ radicals then attack the complex structure of the Congo red dye, leading to its degradation through various pathways, including cleavage of the azo bond (-N=N-) and oxidation of aromatic rings [74].

Comparative study: The synthesized Co_3O_4 nanoparticles demonstrated superior performance as compared to commercially available photocatalysts such as ZnO and TiO_2 (P25)

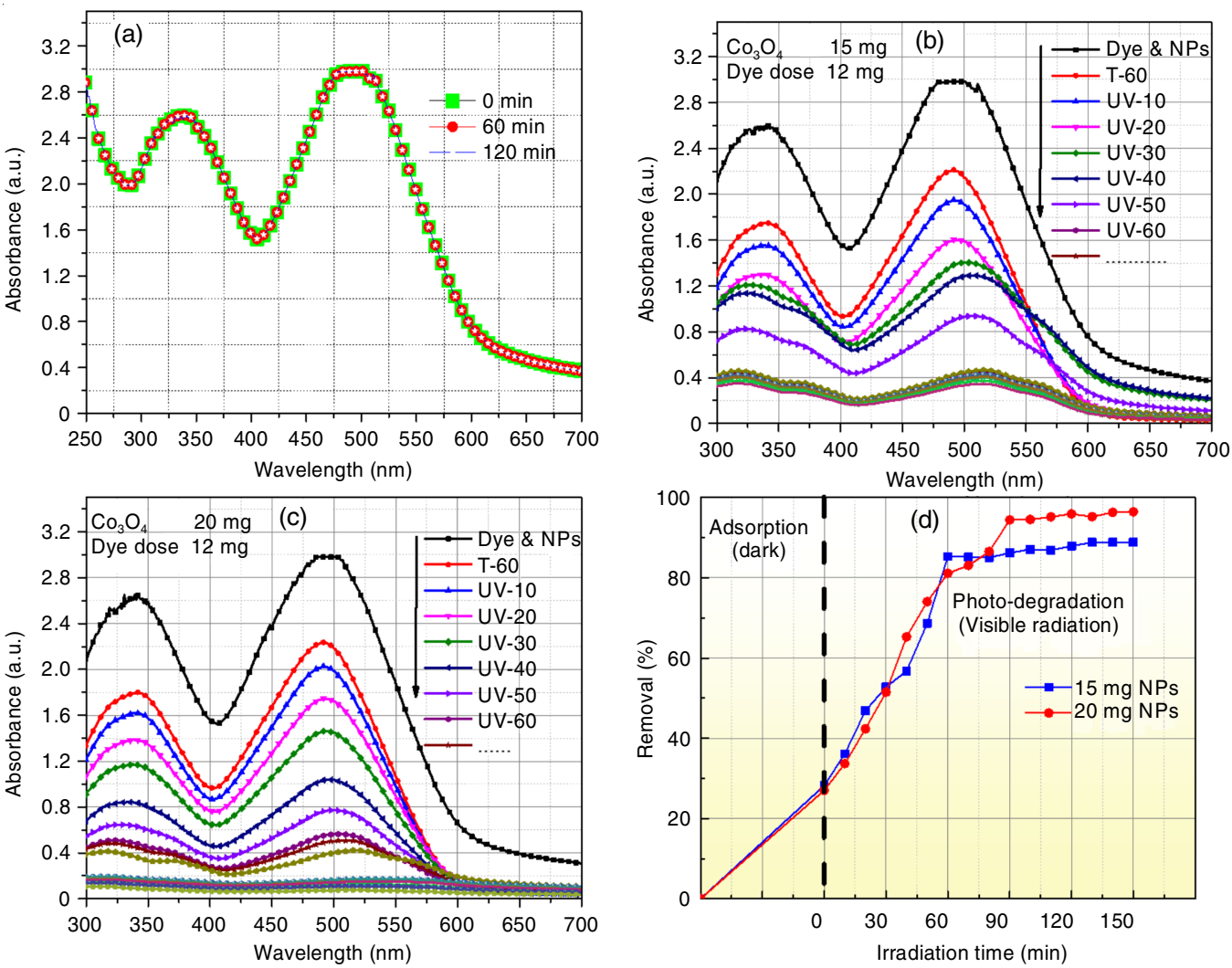

Fig. 7. Degradation of Congo red dye (a) without Co_3O_4, (b) 150 mg L^{-1}, (c) 200 mg L^{-1} and (d) Removal efficiency *vs.* dosage

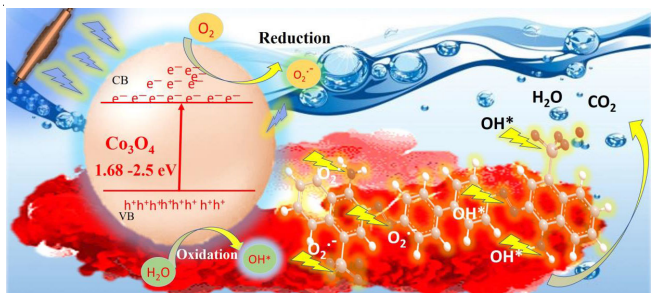

Fig. 8. Schematic of degradation of Congo red dye dye *via* PEG/Co_3O_4 NPs

for the degradation of Congo red dye (Fig. 9). This superior perfor-mance can be attributed to several factors, for example (a) smaller crystallite size, which translates to a larger surface area, providing more active sites for photocatalytic reactions [75,76]; (b) lower band gap energy facilitates the generation of more electron-hole pairs (e^-/h^+) pairs under UV light, ultimately enhancing photocatalytic activity [77] and (c) presence of specific functional groups introduced onto the surface of the PEG-mediated Co_3O_4 nanoparticles may promote adsorption and degradation of Congo red dye molecules by providing additional catalytic sites or improving the interaction between the dye and the photocatalyst [78]. The observed dependence on dosage and superior performance highlights the potential of these nanoparticles for wastewater treatment and environmental remediation applications.

Conclusion

This study presents a novel synthetic method for Co_3O_4 nanoparticles utilizing polyethylene glycol (PEG) as a capping and directing agent. The combined precipitation-cum-hydrothermal approach offers several advantages including (a) enhanced control over morphology which was confirmed through FTIR analysis about the interaction between PEG and Co_3O_4 suggesting the PEG's role in stabilizing and shaping the nanoparticles. The FESEM and HRTEM micrographs revealed unique multi-structured morphologies, unlike conventional spherical Co_3O_4 nanoparticles. (b) The UV-vis spectroscopy reveals two distinct bandgap transitions at 1.68 and 2.5 eV suggesting the influence of PEG on the electronic structure of Co_3O_4. This tunability is crucial for enhancing light absorption and photocatalytic activity in the targeted wavelength range. Remarkably, PEG-mediated Co_3O_4 nanoparticles demonstrated exceptional photocatalytic

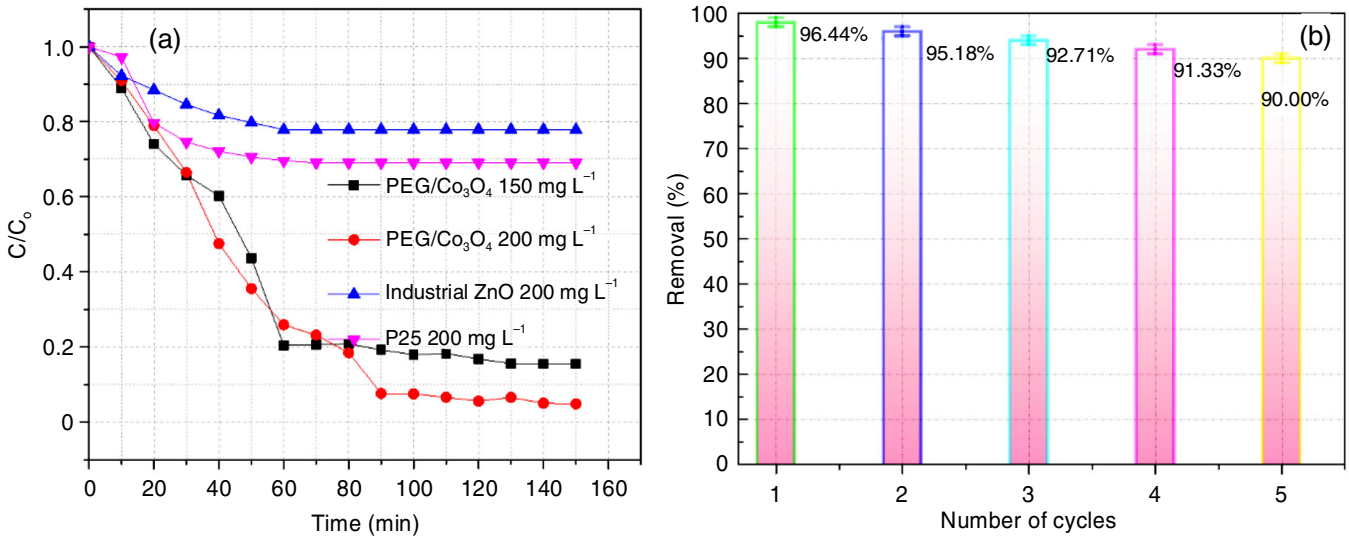

Fig. 9. Degradation analysis of Congo red (CR) dye using PEG/Co_3O_4 nanoparticles: (a) comparative studies and (b) reusability efficiency

performance, achieving nearly complete Congo red dye degradation (96.44%) within 150 min of UV irradiation. This work paves the way for systematic polymer-assisted synthesis of Co_3O_4 nanoparticles with diverse morphologies and tenable electronic properties.

CONFLICT OF INTEREST

The authors declare that there is no conflict of interests regarding the publication of this article.

REFERENCES

1. Q. Liu, Pollution and Treatment of Dye Waste-Water, *IOP Conf. Ser. Earth Environ. Sci.*, **514**, 052001 (2020); https://doi.org/10.1088/1755-1315/514/5/052001
2. D.A. Yaseen and M. Scholz, *Int. J. Environ. Sci. Technol.*, **16**, 1193 (2019); https://doi.org/10.1007/s13762-018-2130-z
3. L. He, F. Michailidou, H.L. Gahlon and W. Zeng, *Chem. Res. Toxicol.*. **35**, 901 (2022); https://doi.org/10.1021/acs.chemrestox.1c00427
4. B. Lellis, C.Z. Fávaro-Polonio, J.A. Pamphile and J.C. Polonio, *Biotechnol. Res. Innov.*, **3**, 275 (2019); https://doi.org/10.1016/j.biori.2019.09.001
5. C.V. Nachiyar, A.D. Rakshi, S. Sandhya, N.B.D. Jebasta and J. Nellore, *Case Stud. Chem. Environ. Eng.*, **7**, 100339 (2023); https://doi.org/10.1016/j.cscee.2023.100339
6. A.K.D. Alsukaibi, *Processes*, **10**, 1968 (2022); https://doi.org/10.3390/pr10101968
7. B. Sarkodie, J. Amesimeku, C. Frimpong, E.K. Howard, Q. Feng and Z. Xu, *Chemosphere*, **313**, 137654 (2023); https://doi.org/10.1016/j.chemosphere.2022.137654
8. M. Pavel, C. Anastasescu, R.-N. State, A. Vasile, F. Papa and I. Balint, *Catalysts*, **13**, 380 (2023); https://doi.org/10.3390/catal13020380
9. G. Ren, H. Han, Y. Wang, S. Liu, J. Zhao, X. Meng and Z. Li, *Nanomaterials*, **11**, 1804 (2021); https://doi.org/10.3390/nano11071804
10. R. Vinayagam, P. Senthil Kumar, G. Rangasamy, T. Varadavenkatesan, A. Hebbar, G. Murugesan, S. Srivastava, L.C. Goveas, N. Manoj Kumar and R. Selvaraj, *Environ. Res.*, **216**, 114766 (2022); https://doi.org/10.1016/j.envres.2022.114766
11. S. Kumar, G. Kaur, M. Rawat, Y.F. Tsang, K.-Y. Lin and K.-H. Kim, *J. Clean. Prod.*, **361**, 132242 (2022); https://doi.org/10.1016/j.jclepro.2022.132242
12. A.M. Abdallah and R. Awad, *J. Supercond. Nov. Magn.*, **33**, 1395 (2020); https://doi.org/10.1007/s10948-019-05296-1
13. T. Ozkaya, A. Baykal, M.S. Toprak, Y. Koseoglu and Z. Durmus, *J. Magn. Magn. Mater.*, **321**, 2145 (2009); https://doi.org/10.1016/j.jmmm.2009.01.003
14. C.I. Priyadharsini, G. Marimuthu, T. Pazhanivel, P.M. Anbarasan, V. Aroulmoji, V. Siva and L. Mohana, *J. Sol-Gel Sci. Technol.*, **96**, 416 (2020); https://doi.org/10.1007/s10971-020-05393-x
15. D.Y. Kim, S.H. Ju, H.Y. Koo, S.K. Hong and Y.C. Kang, *J. Alloys Compd.*, **417**, 254 (2006); https://doi.org/10.1016/j.jallcom.2005.09.013
16. A. UmaSudharshini, M. Bououdina, M. Venkateshwarlu, C. Manoharan and P. Dhamodharan, *Surf. Interfaces*, **19**, 100535 (2020); https://doi.org/10.1016/j.surfin.2020.100535
17. C. Karuppiah, B. Thirumalraj, S. Alagar, S. Piraman, Y.-J.J. Li and C.-C. Yang, *Catalysts*, **11**, 76 (2021); https://doi.org/10.3390/catal11010076
18. M. Yarestani, A.D. Khalaji, A. Rohani and D. Das, *J. Sci. Islamic Republic of Iran*, **25**, 339 (2014).
19. D. Bokov, A. Turki Jalil, S. Chupradit, W. Suksatan, M. Javed Ansari, I.H. Shewael, G.H. Valiev and E. Kianfar, *Adv. Mater. Sci. Eng.*, **2021**, 5102014 (2021); https://doi.org/10.1155/2021/5102014
20. M. Khalil, J. Yu, N. Liu and R.L. Lee, *J. Nanopart. Res.*, **16**, 2362 (2014); https://doi.org/10.1007/s11051-014-2362-x
21. H.M. Saleh and A.I. Hassan, *Sustainability*, **15**, 10891 (2023); https://doi.org/10.3390/su151410891
22. J.A. Darr, J. Zhang, N.M. Makwana and X. Weng, *Chem. Rev.*, **117**, 11125 (2017); https://doi.org/10.1021/acs.chemrev.6b00417
23. M. Escamilla, K. Pachuta, K. Huang, M. Klingseisen, H. Cao, H. Zhang, A. Sehirlioglu and E. Pentzer, *Mater. Adv.*, **3**, 2354 (2022); https://doi.org/10.1039/D1MA00832C
24. A.F. Khusnuriyalova, M. Caporali, E. Hey-Hawkins, O.G. Sinyashin and D.G. Yakhvarov, *Eur. J. Inorg. Chem.*, **2021**, 3023 (2021); https://doi.org/10.1002/ejic.202100367
25. R. Javed, A. Sajjad, S. Naz, H. Sajjad and Q. Ao, *Int. J. Mol. Sci.*, **23**, 10521 (2022); https://doi.org/10.3390/ijms231810521
26. R. Javed, M. Zia, S. Naz, S.O. Aisida, N. Ain and Q. Ao, *J. Nanobiotechnol.*, **18**, 172 (2020); https://doi.org/10.1186/s12951-020-00704-4
27. Y. Köseoglu, A. Baykal, M.S. Toprak, F. Gözüak, A.C. Basaran and B. Aktas, *J. Alloys Compd.*, **462**, 209 (2008); https://doi.org/10.1016/j.jallcom.2007.07.121

28. A. Jose, K.R. Sunaja Devi, D. Pinheiro and S.L. Narayana, *J. Photochem. Photobiol. B*, **187**, 25 (2018); https://doi.org/10.1016/j.jphotobiol.2018.07.022
29. M. Anandan, S. Dinesh, N. Krishnakumar and K. Balamurugan, *J. Mater. Sci. Mater. Electron.*, **27**, 12517 (2016); https://doi.org/10.1007/s10854-016-5764-y
30. M. Zhang, J. Lei, Y. Shi, L. Zhang, Y. Ye, D. Li and C. Mu, *RSC Adv.*, **6**, 83366 (2016); https://doi.org/10.1039/C6RA12988A
31. J. Lei, L. Deng, X. Li, Y. Xu, D. Li and C. Mu, *Environ. Sci. Pollut. Res. Int.*, **25**, 26259 (2018); https://doi.org/10.1007/s11356-018-2679-6
60. M. Farahmandjou, *Phys. Chem. Res.*, **4**, 153 (2016); https://doi.org/10.22036/PCR.2016.12909
51. S. Farhadi, M. Javanmard and G. Nadri, *Acta Chim. Slov.*, **63**, 335 (2016); https://doi.org/10.17344/acsi.2016.2305
32. M.M. Rahman, J.-Z. Wang, X.-L. Deng, Y. Li and H.-K. Liu, *Electrochim. Acta*, **55**, 504 (2009); https://doi.org/10.1016/j.electacta.2009.08.068
33. A. Askarinejad and A. Morsali, *Ultrason. Sonochem.*, **16**, 124 (2009); https://doi.org/10.1016/j.ultsonch.2008.05.015
34. C. Dong, X. Xiao, G. Chen, H. Guan and Y. Wang, *Mater. Chem. Phys.*, **155**, 1 (2015); https://doi.org/10.1016/j.matchemphys.2015.01.033
35. A.M. Abdallah and R. Awad, *Physica B*, **608**, 412898 (2021); https://doi.org/10.1016/j.physb.2021.412898
36. M. Christy, M.R. Jisha, A.R. Kim, K.S. Nahm, D.J. Yoo, E.K. Suh, T.S. Devi Kumari, T. Prem Kumar and A.M. Stephan, *Bull. Korean Chem. Soc.*, **32**, 1204 (2011); https://doi.org/10.5012/bkcs.2011.32.4.1204
37. C. Luo, Y. Zhang, X. Zeng, Y. Zeng and Y. Wang, *J. Colloid Interface Sci.*, **288**, 444 (2005); https://doi.org/10.1016/j.jcis.2005.03.005
38. N. Rai and S. Kanagaraj, *ACS Omega*, **26**, 22363 (2022); https://doi.org/10.1021/acsomega.2c01266
39. R. Abbasi, G. Shineh, M. Mobaraki, S. Doughty and L. Tayebi, *J. Nanopart. Res.*, **25**, 43 (2023); https://doi.org/10.1007/s11051-023-05690-w
40. R. Bhargava, S. Khan, N. Ahmad and M.M.N. Ansari, *AIP Conf. Proc.*, **1953**, 030034 (2018); https://doi.org/10.1063/1.5032369
41. T. He, D. Chen, X. Jiao, Y. Wang and Y. Duan, *Chem. Mater.*, **17**, 4023 (2005); https://doi.org/10.1021/cm050727s
42. S. Dubey, J. Kumar, A. Kumar and Y.C. Sharma, *Adv. Powder Technol.*, **29**, 2583 (2018); https://doi.org/10.1016/j.apt.2018.03.009
43. P. Lokanatha Reddy, K. Deshmukh, K. Chidambaram, B. Ahamed, K. Kumar Sadasivuni, D. Ponnamma, R. Lakshmipathy, D. Dayananda and S.K. Khadheer Pasha, *Mater. Today Proc.*, **9**, 175 (2019); https://doi.org/10.1016/j.matpr.2019.02.150
44. Y. Yang, J. Liang, W. Jin, Y. Li, M. Xuan, S. Wang, X. Sun, C. Chen and J. Zhang, *RSC Adv.*, **10**, 14670 (2020); https://doi.org/10.1039/D0RA01307B
45. A. Sarfraz and K. Hasanain, *Acta Phys. Pol. A*, **125**, 139 (2014); https://doi.org/10.12693/APhysPolA.125.139
46. B.M. Abu-Zied and K.A. Alamry, *J. Alloys Compd.*, **798**, 820 (2019); https://doi.org/10.1016/j.jallcom.2019.05.249
47. A. Miura, Y. Uraoka, T. Fuyuki, S. Yoshii and I. Yamashita, *J. Appl. Phys.*, **103**, 074503 (2008); https://doi.org/10.1063/1.2888357
48. K.M. Mohamed, J.J. Benitto, J.J. Vijaya and M. Bououdina, *Crystals*, **13**, 329 (2023); https://doi.org/10.3390/cryst13020329
49. P. Innocenzi, *J. Non-Cryst. Solids*, **316**, 309 (2003); https://doi.org/10.1016/S0022-3093(02)01637-X
50. M. Fernandes Queiroz, K. Melo, D. Sabry, G. Sassaki and H. Rocha, *Mar. Drugs*, **13**, 141 (2014); https://doi.org/10.3390/md13010141
52. M. Sertçelik, *J. Chem. Res.*, **45**, 42 (2021); https://doi.org/10.1177/1747519820924636
53. E.N. Mainsah, S.-J.E. Ntum, M.A. Conde, G.T. Chi, J. Raftery, P.T. Ndifon, *Cryst. Struct. Theor. Appl.*, **8**, 97138 (2019); https://doi.org/10.4236/csta.2019.84004
54. Y. Liu, G. Zhu, B. Ge, H. Zhou, A. Yuan and X. Shen, *CrystEngComm*, **14**, 6264 (2012); https://doi.org/10.1039/c2ce25788b
55. M. Sahu, V.R.M. Reddy, B. Kim, B. Patro, C. Park, W.K. Kim and P. Sharma, *Materials*, **15**, 1708 (2022); https://doi.org/10.3390/ma15051708
56. G. Hitkari, S. Sandhya, P. Gajanan, M.K. Shrivash and D. Kumar, *J. Mater. Sci. Eng.*, **7**, 419 (2018); https://doi.org/10.4172/2169-0022.1000419
57. I. Bibi, N. Nazar, M. Iqbal, S. Kamal, H. Nawaz, S. Nouren, Y. Safa, K. Jilani, M. Sultan, S. Ata, F. Rehman and M. Abbas, *Adv. Powder Technol.*, **28**, 2035 (2017); https://doi.org/10.1016/j.apt.2017.05.008
58. R.R. Samal, A.K. Samantara, S. Mahalik, J.N. Behera, B. Dash and K. Sanjay, *New J. Chem.*, **45**, 2795 (2021); https://doi.org/10.1039/D0NJ05088A
59. A.R. Campanelli and L. Scaramuzza, *Acta Cryst.*, **C42**, 1380 (1986); https://doi.org/10.1107/S0108270186092193
61. Y. Wang, J.-C. Shi, J.-L. Cao, G. Sun and Z.-Y. Zhang, *Mater. Lett.*, **65**, 222 (2011); https://doi.org/10.1016/j.matlet.2010.09.090
62. J. Ahmed, T. Ahmad, K.V. Ramanujachary, S.E. Lofland and A.K. Ganguli, *J. Colloid Interface Sci.*, **321**, 434 (2008); https://doi.org/10.1016/j.jcis.2008.01.052
63. S. Kundu and M. Jayachandran, *J. Nanopart. Res.*, **15**, 1543 (2013); https://doi.org/10.1007/s11051-013-1543-3
64. S. Abouali, M. Akbari Garakani, B. Zhang, Z.-L. Xu, E. Kamali-Heidari, J. Huang, J. Huang and J.-K. Kim, *ACS Appl. Mater. Interfaces*, **7**, 13503 (2015); https://doi.org/10.1021/acsami.5b02787
65. X. Dai, Y. Dai, J. Lu, L. Pu, W. Wang, J. Jin, F. Ma and N. Tie, *Ionics*, **26**, 2501 (2020); https://doi.org/10.1007/s11581-019-03333-6
66. Y. Zhang, X. Zhong, J. Zhu and X. Song, *Nanotechnology*, **18**, 195605 (2007); https://doi.org/10.1088/0957-4484/18/19/195605
67. M. Ghosh, E.V. Sampathkumaran and C.N.R. Rao, *Chem. Mater.*, **17**, 2348 (2005); https://doi.org/10.1021/cm0478475
68. S.-Y. Zhang, T.-T. Li, H.-L. Zhu and Y.-Q. Zheng, *J. Mater. Sci.*, **53**, 4323 (2018); https://doi.org/10.1007/s10853-017-1855-2
69. S. Yamamoto, H. Bluhm, K. Andersson, G. Ketteler, H. Ogasawara, M. Salmeron and A. Nilsson, *J. Phys.: Condens. Matter.*, **20**, 184025 (2008); https://doi.org/10.1088/0953-8984/20/18/184025
70. A.R. Deline, B.P. Frank, C.L. Smith, L.R. Sigmon, A.N. Wallace, M.J. Gallagher, D.G. Goodwin Jr., D.P. Durkin and D.H. Fairbrother, *Chem. Rev.*, **120**, 11651 (2020); https://doi.org/10.1021/acs.chemrev.0c00351
71. P. Parthasarathy, S. Sajjad, J. Saleem, M. Alherbawi and G. Mckay, *Separations*, **9**, 139 (2022); https://doi.org/10.3390/separations9060139
72. K. Sharma, S. Pandit, B.S. Thapa and M. Pant, *Catalysts*, **12**, 1219 (2022); https://doi.org/10.3390/catal12101219
73. A. Kudo and Y. Miseki, **38**, 253 (2009); https://doi.org/10.1039/B800489G
74. I.K. Konstantinou and T.A. Albanis, *Appl. Catal. B*, **49**, 1 (2004); https://doi.org/10.1016/j.apcatb.2003.11.010
75. M.B. Tahir, M. Sohaib, M. Sagir and M. Rafique, *Encyclopedia Smart Mater.*, **2**, 578 (2022); https://doi.org/10.1016/B978-0-12-815732-9.00006-1
76. S.J. Armakovic, M.M. Savanovic and S. Armakovic, *Catalysts*, **13**, 26 (2022); https://doi.org/10.3390/catal13010026
77. H. Chen, C. Xue, D. Cui, M. Liu, Y. Chen, Y. Li and W. Zhang, *RSC Adv.*, **10**, 15245 (2020); https://doi.org/10.1039/C9RA10437B
78. R.S. Reena, A. Aslinjensipriya, M. Jose and S.J. Das, *J. Mater. Sci. Mater. Electron.*, **31**, 22057 (2020); https://doi.org/10.1007/s10854-020-04708-6